Scientific Research Publishing

International Journal of Astronomy and Astrophysics, 2025, 15(2), 65-79
https://www.scirp.org/journal/ijaa
ISSN Online: 2161-4725
ISSN Print: 2161-4717

Discrepancies between Limits and Measurements of Warm Dark Matter Properties

Bruce Hoeneisen

Universidad San Francisco de Quito, Quito, Ecuador
Email: bhoeneisen@usfq.edu.ec

How to cite this paper: Hoeneisen, B. (2025) Discrepancies between Limits and Measurements of Warm Dark Matter Properties. *International Journal of Astronomy and Astrophysics*, **15**, 65-79.
https://doi.org/10.4236/ijaa.2025.152005

Received: March 19, 2025
Accepted: June 14, 2025
Published: June 17, 2025

Abstract

A limit on the expansion parameter $a_{h\mathrm{NR}}$ at which dark matter becomes non-relativistic has been obtained from the observed minimum halo mass hosting Milky Way satellites. This limit is in disagreement with measurements. In the present study, we attempt to understand this disagreement. We find that the limit does not include the following phenomena: non-linear regeneration of the power spectrum of density perturbations, and the stripping of galaxy halos by neighboring galaxies. Considering these phenomena, we find that there is no longer a significant discrepancy between the limit and the measurements.

Keywords

Warm Dark Matter, Galaxy, Galaxy Formation, Dwarf Galaxies

1. Introduction

Most non-relativistic matter in the universe is in a "dark matter" form that has only been "observed" through its gravitational interaction [1]. Let us assume that this dark matter is a gas of a single particle species of mass m_h. The effect of this dark matter on cosmology, under quite general conditions, can be described with a single parameter $a_{h\mathrm{NR}}$ [2] to be added to the six parameters of the standard cold dark matter ΛCDM cosmology [1]. $a_{h\mathrm{NR}}$ is the characteristic universe expansion factor $a(t)$ at which the dark matter particles become non-relativistic. $a(t)$ is normalized so that $a(t_0)=1$ at the present time t_0. Several estimated limits on $a_{h\mathrm{NR}}$ have been summarized in Table 3 of [2]. The limits are

$$a_{h\mathrm{NR}} < 6\times 10^{-5} \tag{1}$$

from Big Bang Nucleosynthesis (BBN) observations,

$$a_{h\mathrm{NR}} \lesssim 7\times10^{-6} \tag{2}$$

from observed Cosmic Microwave Background (CMB) radiation fluctuations,

$$a_{h\mathrm{NR}} \lesssim 7\times10^{-7} \tag{3}$$

from observations of the Lyman-α forest of quasar light, and

$$a_{h\mathrm{NR}} \lesssim 6\times10^{-8} \tag{4}$$

from the observed population of small galaxy halos. In contrast, $a_{h\mathrm{NR}}$ has been *measured* with dwarf galaxy rotation curves [3] [4]:

$$a_{h\mathrm{NR}} = (1.39 \pm 0.24)\times10^{-6}. \tag{5}$$

There is a discrepancy between (4) and (5). Each of these measurements and limits has its own issues. The purpose of the present study is to try to understand the discrepancy between (4) and (5).

The general conditions mentioned above assume dark matter with or without interactions with the Standard Model sector or self-interactions, as long as the chemical potential is non-positive. In the present study, we further assume that dark matter was once in thermal equilibrium with the early Standard Model sector, *i.e.* we consider "thermal relic" dark matter.

The limit (4) is obtained from the minimum halo mass hosting Milky Way satellites [2], [5]-[13]:

$$M_h < 5.4\times10^8\ \mathrm{M}_\odot, \tag{6}$$

at 2σ confidence [2]. The corresponding observed stellar mass is of order $M_* \approx 10^5\ \mathrm{M}_\odot$ [2] (that agrees with the calculation in [14]). The authors of [2] state that (4) is an *estimate*, and, due to non-linearities, "should be more rigorously studied by cosmological simulation". Below we fill in this gap.

The present work is a continuation of [15] and [16]. These references may be consulted for details. To make the present article self-contained we list some definitions in Section 2. Warm dark matter introduces the "free-streaming cut-off" discussed in Section 3. Numerical integration of hydrodynamical equations is presented in Section 4. The non-linear regeneration of small scale structure is discussed in Section 5, and the bottom-up and top-down evolution of structure in the warm dark matter scenario is presented in Section 6. Conclusions follow.

2. Definitions

We use the notation and parameter values of [1]. Our definitions follow. Let $v_{h\mathrm{rms}}(a)$ be the 3-D root-mean-square thermal velocity of non-relativistic warm dark matter particles at expansion parameter $a(t)$ when the universe is nearly homogeneous. $v_{h\mathrm{rms}}(a)$ scales as a^{-1}, so

$$v_{h\mathrm{rms}}(1) = a\cdot v_{h\mathrm{rms}}(a) \tag{7}$$

is an adiabatic invariant, and

$$a_{h\mathrm{NR}} \equiv 1.03\frac{v_{h\mathrm{rms}}(1)}{c}, \tag{8}$$

where 1.03 is a threshold factor for bosons (0.98 for fermions) [4]. Warm dark matter free-streaming attenuates the *linear* power spectrum of density perturbations $P_{\mathrm{CDM}}(k)$ of the ΛCDM cosmology, at large comoving wavevector k, by a factor [17]

$$\tau^2(k) \equiv \frac{P_{\mathrm{WDM}}(k)}{P_{\mathrm{CDM}}(k)} = \left[1+(\alpha k)^{2\nu}\right]^{-10/\nu}, \tag{9}$$

where $\nu = 1.12$, and

$$\alpha = 0.049\left(\frac{m_h}{1\,\mathrm{keV}}\right)^{-1.11}\left(\frac{\Omega_c}{0.25}\right)^{0.11}\left(\frac{h}{0.7}\right)^{1.22}\frac{1}{h}\mathrm{Mpc}. \tag{10}$$

These equations, often used in the literature, *define* the "standard thermal relic mass" m_h. Limits in the literature often obtain a lower bound to this m_h. The actual dark matter particle mass is model-dependent, see Table 4 of [4]. Equation (9) can be approximated by

$$\tau^2(k) \approx \exp\left(-\frac{k^2}{k_{\mathrm{fs}}^2}\right), \text{ where } k_{\mathrm{fs}} = \frac{1}{2.59\cdot\alpha}, \tag{11}$$

except for a "tail" to be discussed below. k_{fs} is the comoving free-streaming wavevector. At this wavevector, $\tau^2(k_{\mathrm{fs}}) = 1/e$ (other definitions in the literature are 1/2 or 1/4). An effective warm dark matter comoving free-streaming length can be defined as

$$l_{\mathrm{fs}} = 0.26\frac{2\pi}{k_{\mathrm{fs}}}, \tag{12}$$

where the factor 0.26 comes from an integration over angles. l_{fs} is approximately proportional to $v_{h\mathrm{rms}}(1)$:

$$l_{\mathrm{fs}} \approx 4.9\left[\frac{\mathrm{Mpc}}{\mathrm{km/s}}\right]\cdot v_{h\mathrm{rms}}(1). \tag{13}$$

An analytic expression that relates directly $v_{h\mathrm{rms}}(1)$ and k_{fs} (that does not include free-streaming during radiation domination while inside the horizon) is [18] [19]

$$k_{\mathrm{fs}}(t_{\mathrm{eq}}) = \frac{1.455}{\sqrt{2}}\sqrt{\frac{4\pi G\Omega_m\rho_{\mathrm{crit}}a_{\mathrm{eq}}}{v_{h\mathrm{rms}}^2(1)}}. \tag{14}$$

This comoving wavevector approximately separates growing from decaying modes at the time t_{eq} of equal radiation and matter densities. Thereafter, k_{fs} grows as $\propto a^{1/2}$, allowing regeneration of small scale structure, giving $\tau(k)$ a "tail" that depends on $a(t)$. The 3-D Fourier transform of (11) defines a linear free-streaming mass scale

$$M_{\mathrm{fs}} \approx \frac{4}{3}\pi\left(\frac{1.555}{k_{\mathrm{fs}}}\right)^3\Omega_m\rho_{\mathrm{crit}}, \tag{15}$$

where $\Omega_m\rho_{\mathrm{crit}}$ is the present mean matter density of the universe. In conclusion, each of the observables m_h, k_{fs}, l_{fs}, $v_{h\mathrm{rms}}(1)$, $a_{h\mathrm{NR}}$ and M_{fs} deter-

mines all the others.

Astronomers obtain the galaxy "stellar mass" M_* and "halo mass" M_h (also called "virial mass", which is a missnomer in view of [20]). The "halo mass" M_h is often defined as the galaxy mass contained inside a radius r_{200} at which the dark matter density reaches 200 times the mean dark matter density of the universe at the observed redshift of the galaxy [21]. The galaxy stellar mass M_* is obtained from measurements of the relative luminosities of the galaxy with several filters, the measurement of its redshift, and from stellar synthesis models. The galaxy halo mass M_h is *estimated* from M_*, stellar images, (warm) dark matter simulations and abundance matching [21], or exceptionally, with gravitational lensing measurements [20].

3. The Linear Theory

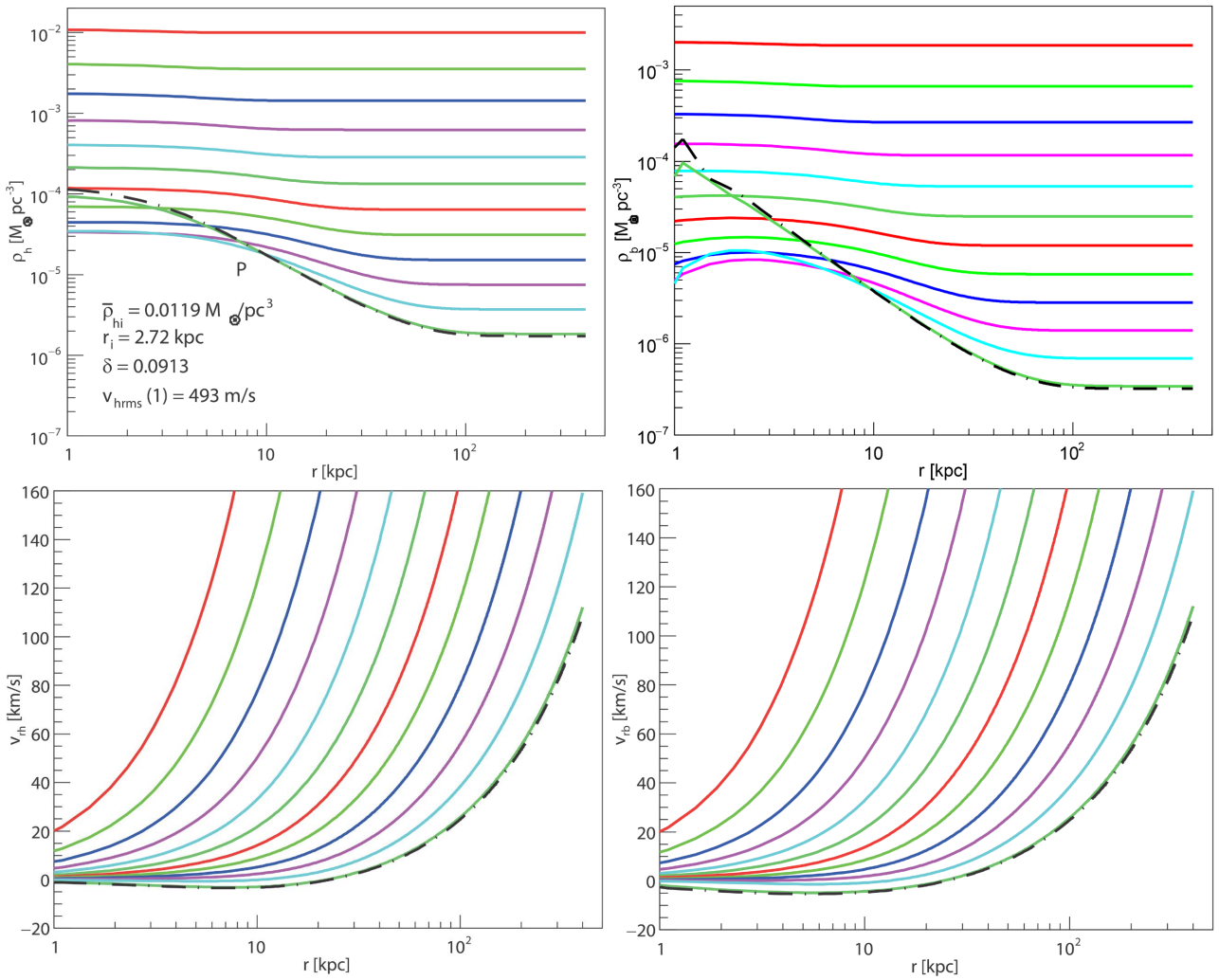

Figure 1. The dark matter and baryon densities and radial velocities, are shown as a function of the proper radius r, at times that increase by factors $\sqrt{2}$ (except for the last dashed line). The initial redshift of the numerical integration is $z_i = 65.9$. The parameters of this simulation are $\bar{\rho}_{hi} = 0.0119\ \mathrm{M}_\odot/\mathrm{pc}^3$, proper $r_i = 2.72$ kpc, $\delta = 0.0913$, and $v_{hrms}(1) = 493$ m/s. The pivot point P has $r_{hP} = 9$ kpc and $\rho_{hP} = 2\times10^{-5}\ \mathrm{M}_\odot/\mathrm{pc}^3$. $M_{PS} = 10^9\ \mathrm{M}_\odot$. $M_h = 3\times10^8\ \mathrm{M}_\odot$. $\sigma(M_{PS}, z_i, k_{fs}) = 0.038$. $V_{rot} = 9.4$ km/s.

The Press-Schechter prediction [22], or its Sheth-Tormen extensions [23] [24], depend on the variance of the relative density perturbation $\delta(\mathbf{x}) \equiv (\rho(\mathbf{x}) - \bar{\rho})/\bar{\rho}$ on the linear total (dark matter plus baryon) mass scale M_{PS}, at redshift z [14] [25]:

$$\sigma^2(M_{\mathrm{PS}}, z, k_{\mathrm{fs}}) = \frac{f^2}{(2\pi)^3 (1+z)^2} \int_0^\infty 4\pi k^2 \mathrm{d}k\, P_{\mathrm{CDM}}(k) \tau^2(k) W^2(k), \tag{16}$$

and so depends on the free-streaming cut-off factor $\tau^2(k)$, and on the window function $W(k)$ that defines the linear mass scale M_{PS}. For a Gaussian window function

$$W(k) = \exp\left(-\frac{k^2}{2k_0^2}\right) \text{ and } M_{\mathrm{PS}} = \frac{4}{3}\pi \left(\frac{1.555}{k_0}\right)^3 \Omega_m \rho_{\mathrm{crit}}. \tag{17}$$

We calibrate the amplitude of $P_{\mathrm{CDM}}(k)$ with $\sigma_8 = 0.811$ [1] with a "top-hat" window function of radius $8/h$ Mpc, and $f = 1$. For our examples of Section 4, we take $f = 1/0.79$ due to the recent accelerated expansion of the universe [14]. The resulting predictions of the galaxy stellar mass distributions with $M_{\mathrm{PS}} \approx 10^{1.5} M_*$, and the galaxy ultra-violet luminosity distributions, are excellent in a wide range of redshifts z (provided $\tau(k)$ acquires a "tail" discussed in Section 6 below), see, for example [26].

4. Galaxy Formation

The formation of a galaxy with warm dark matter and baryons is described by hydrodynamical equations [15]. These equations are valid for collisionless, or collisional warm dark matter particles, so long as collisions are elastic. A numerical integration of these hydrodynamical equations is presented in **Figure 1**, assuming spherical symmetry. We are interested in the limit of very small dark matter particle mass and large velocity dispersion, so, for all examples in this article, we choose

$$m_h = 0.15 \text{ keV} \text{ and } v_{h\mathrm{rms}}(1) = 493 \text{ m/s}. \tag{18}$$

This particular choice of parameters is justified in Table 4 of [4]. According to (8), (10) and (12) the comoving free-streaming cut-off wavevector is $k_{\mathrm{fs}} \approx 0.67$ Mpc^{-1}, the comoving effective free-streaming length is $l_{\mathrm{fs}} \approx 2.4$ Mpc, and the dark matter becomes non-relativistic at the expansion parameter $a_{h\mathrm{NR}} \approx 1.7 \times 10^{-6}$. Note that this $a_{h\mathrm{NR}}$ is in agreement with the measurement (5), and in disagreement with the limit (4). The linear total (dark matter plus baryon) mass corresponding to k_{fs} is $M_{\mathrm{fs}} \approx 2 \times 10^{12}\, \mathrm{M}_\odot$.

The numerical integration in **Figure 1** begins at redshift $z_i = 65.9$, with initial dark matter and baryon densities

$$\rho_{hi}(r) = \frac{\Omega_h}{\Omega_b} \rho_{bi}(r) = \langle \bar{\rho}_{hi} \rangle \left[1 + \delta \exp\left(-r^2/r_i^2\right)\right], \tag{19}$$

with $\langle \bar{\rho}_{hi} \rangle = 0.0119\, \mathrm{M}_\odot/\mathrm{pc}^3$ (corresponding to z_i), $r_i = 2.72$ kpc and $\delta = 0.0913$. The initial velocities are $v_{hi}(r) = v_{bi}(r) = H(t_i) r$ (and a tiny cor-

rection due to δ). The linear "Press-Schechter" mass corresponding to r_i is $M_{\mathrm{PS}} = 10^9\ \mathrm{M}_\odot$, and the relative mass fluctuation on this mass scale at z_i is $\sigma = 0.038$. The subscript h stands for dark matter, and the subscript b stands for "baryons".

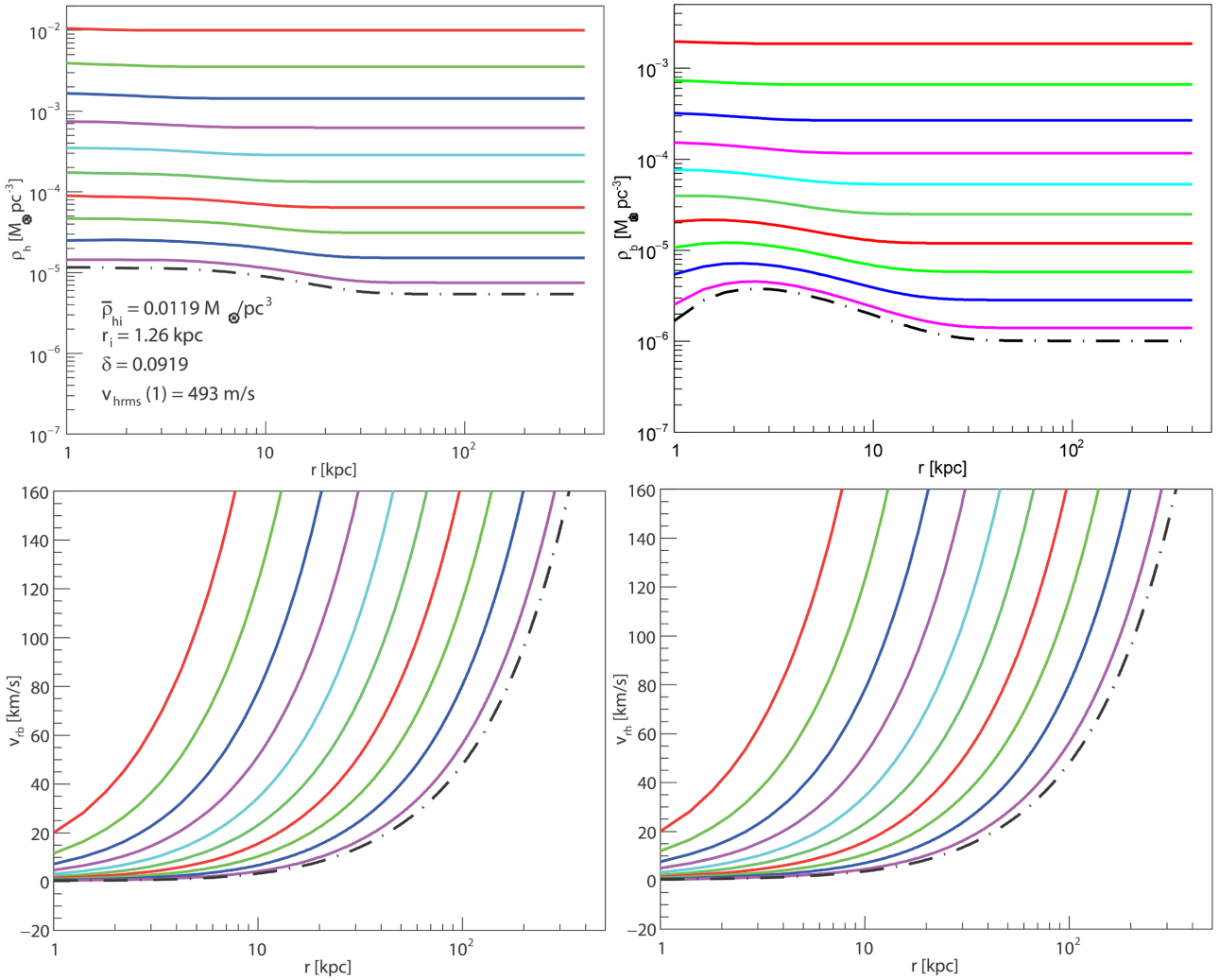

Figure 2. The dark matter and baryon densities and radial velocities are shown as a function of the proper radius r, at times that increase by factors $\sqrt{2}$ (except the last dashed curve). The initial redshift of the numerical integration is $z_i = 65.9$. The parameters of this simulation are $\bar{\rho}_{hi} = 0.0119\ \mathrm{M}_\odot/\mathrm{pc}^3$, $r_i = 1.26$ kpc, $\delta = 0.092$, and $v_{hrms}(1) = 493$ m/s. There is no pivot point P, so no galaxy halo forms. $M_{\mathrm{PS}} = 10^8\ \mathrm{M}_\odot$. $\sigma(M_{\mathrm{PS}}, z_i, k_{\mathrm{fs}}) = 0.038$.

A moment past the last time presented in **Figure 1**, the density $\rho_h(r)$ becomes a "cored isothermal sphere" [15] [16], *i.e.* a solution of the static limit of the hydrodynamical equations, with a density run $\rho_h(r) \propto r^{-2}$ at $r \gg r_c$, and a core radius

$$r_c = \sqrt{\frac{\langle v_{hr}^2 \rangle}{2\pi G \rho_{hc}}}, \tag{20}$$

with the root-mean-square dark matter radial velocity

$$\sqrt{\left\langle v_{hr}^2 \right\rangle} \approx \frac{v_{hrms}(1)}{\sqrt{3}} \left(\frac{\rho_{hc}}{\Omega_c \rho_{crit}} \right)^{1/3}, \tag{21}$$

that is independent of r and t [16]. The radius of the isothermal sphere keeps growing due to the expansion of the universe [16].

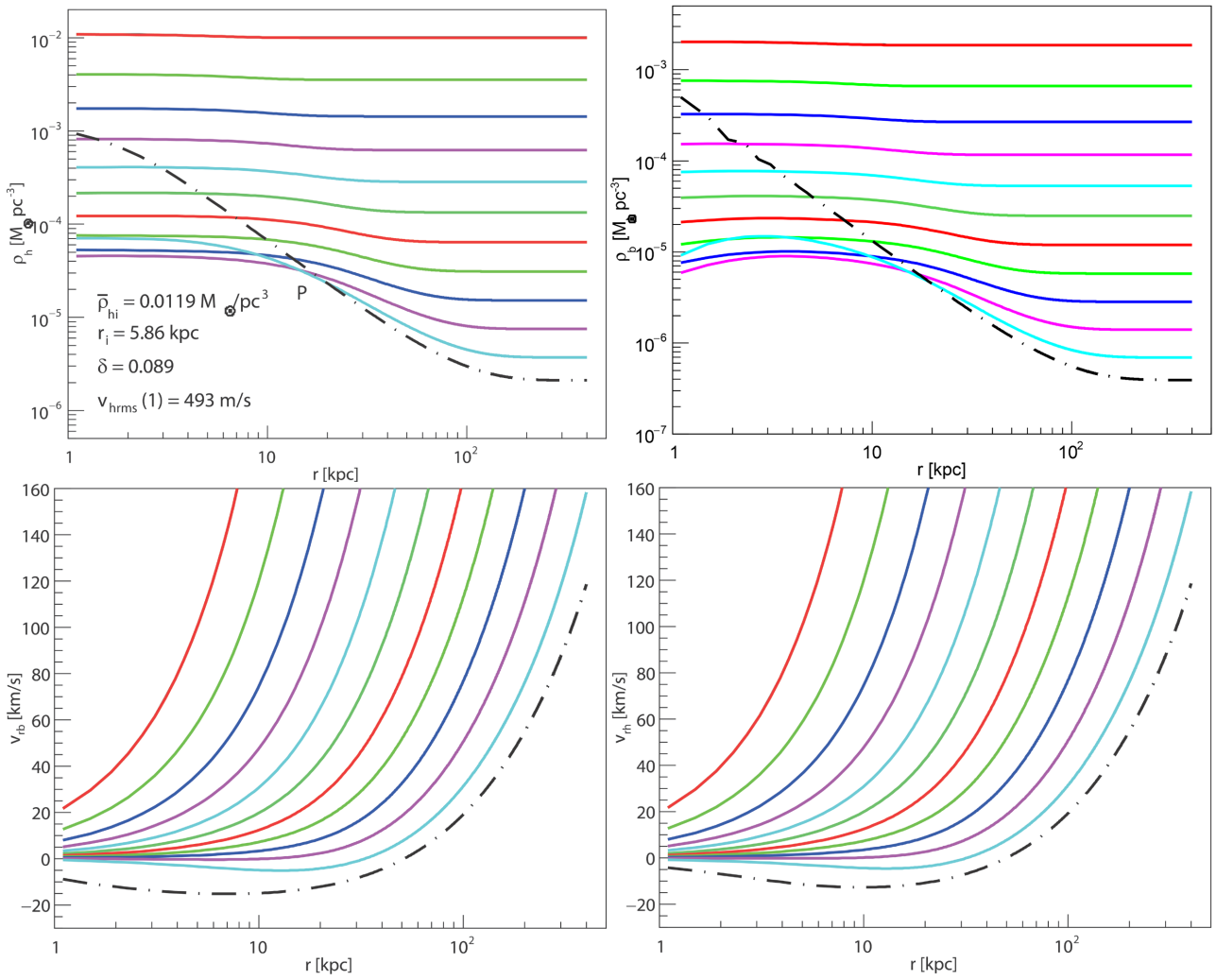

Figure 3. The dark matter and baryon densities and radial velocities are shown as a function of the proper radius r, at times that increase by factors $\sqrt{2}$ (except for the last dashed line). The initial redshift of the numerical integration is $z_i = 65.9$. The parameters of this simulation are $\bar{\rho}_{hi} = 0.0119\ \mathrm{M}_\odot/\mathrm{pc}^3$, $r_i = 5.86$ kpc, $\delta = 0.089$, and $v_{hrms}(1) = 493$ m/s. The pivot point P has $r_{hP} = 17$ kpc and $\rho_{hP} = 2.3\times10^{-5}\ \mathrm{M}_\odot/\mathrm{pc}^3$. $M_{PS} = 10^{10}\ \mathrm{M}_\odot$. $M_h = 3\times10^9\ \mathrm{M}_\odot$. $\sigma(M_{PS}, z_i, k_{fs}) = 0.037$. $V_{rot} = 19$ km/s.

The numerical integration of **Figure 1** obtains the "pivot point" P with $r_{hP} = 9$ kpc and $\rho_{hP} = 2\times10^{-5}\ \mathrm{M}_\odot/\mathrm{pc}^3$. From these numbers, we obtain the radius at which the dark matter halo density is 200 times the present mean dark matter density of the universe (since satellites of the Milky Way are observed at $z \approx 0$): $r_{200} = 16$ kpc, and the corresponding halo mass

$$M_h \equiv M_{200} = \frac{2\langle v_{hr}^2 \rangle}{G} r_{200} = 3\times 10^8\ \mathrm{M}_\odot. \tag{22}$$

This is the mass that needs to be compared to the minimum observed halo mass (6) [21]. Note that

$$\rho_h(r) r^2 = \rho_{hc} r_c^2 = \rho_{hP} r_{hP}^2 = 200\Omega_c \rho_{\mathrm{crit}} r_{200}^2, \tag{23}$$

and

$$\sqrt{\langle v_{hr}^2 \rangle} = \sqrt{2\pi G \rho_{hP} r_{hP}^2}. \tag{24}$$

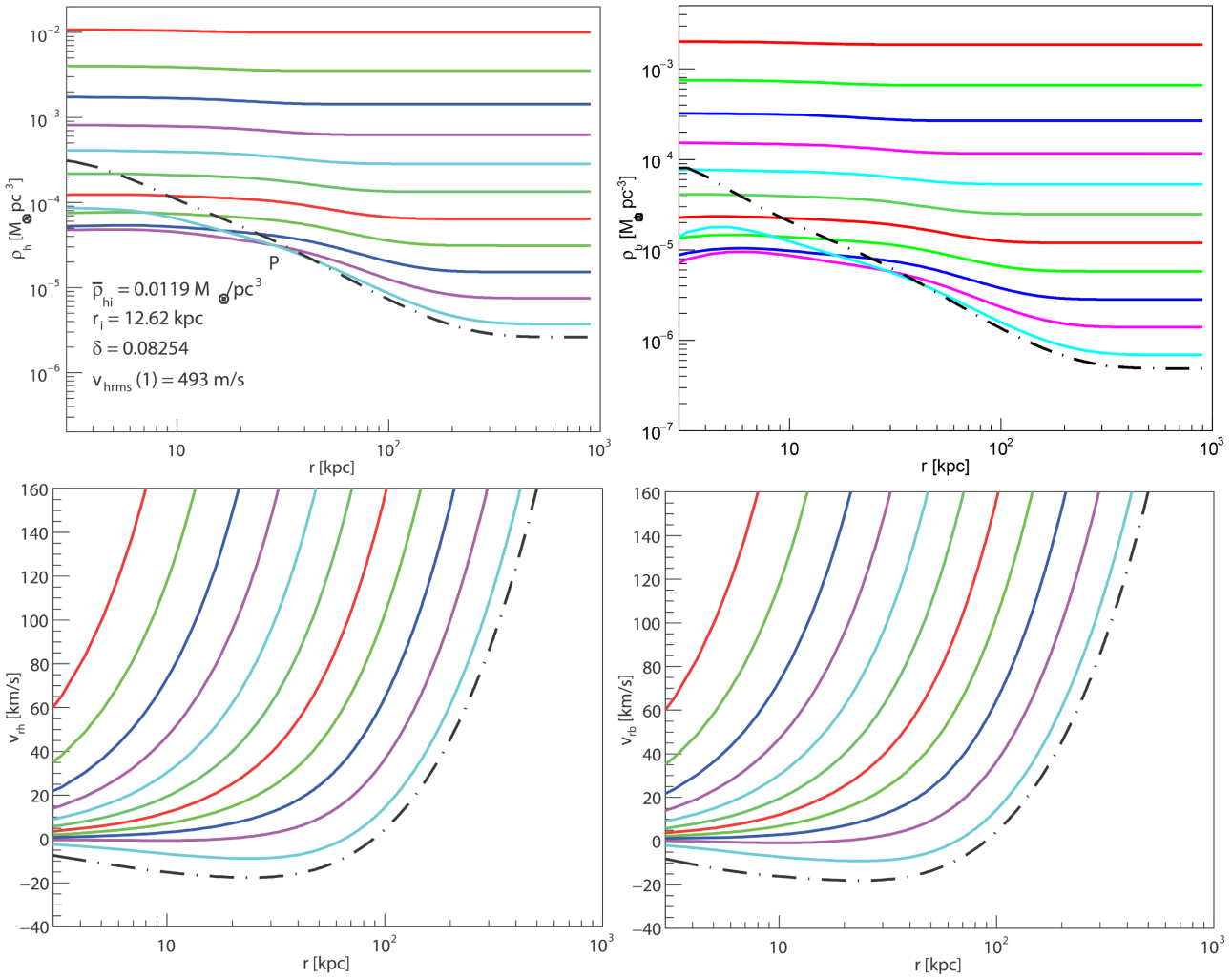

Figure 4. The dark matter and baryon densities and radial velocities are shown as a function of the proper radius r, at times that increase by factors $\sqrt{2}$ (except the last dashed line). The initial redshift of the numerical integration is $z_i = 65.9$. The parameters of this simulation are $\bar{\rho}_{hi} = 0.0119\ \mathrm{M}_\odot/\mathrm{pc}^3$, $r_i = 12.625$ kpc, $\delta = 0.08254$, and $v_{hrms}(1) = 493$ m/s. The pivot point P has $r_{hP} = 35$ kpc and $\rho_{hP} = 2.5\times 10^{-5}\ \mathrm{M}_\odot/\mathrm{pc}^3$. $M_{PS} = 10^{11}\ \mathrm{M}_\odot$. $M_h = 3\times 10^{10}\ \mathrm{M}_\odot$. $\sigma(M_{PS}, z_i, k_{fs}) = 0.036$. $V_{rot} = 41$ km/s.

The origin of the core is explained in [16], and is of cosmological origin, see (21). In the example of **Figure 1**, the core radius and density are $r_c = 2.0$ kpc and

$\rho_{hc} = 4\times10^{-4}\ \mathrm{M}_\odot/\mathrm{pc}^3$. $\sqrt{\langle v_{hr}^2\rangle} = 6.6$ km/s, so the velocity of rotation of a test particle is $V_{\mathrm{rot}} = \sqrt{2\langle v_{hr}^2\rangle} = 9.4$ km/s. This is a "small" galaxy indeed!

The simulation for $M_{\mathrm{PS}} = 10^8\ \mathrm{M}_\odot$, with the listed parameters, does not form a halo, see **Figure 2**. Simulations of more massive galaxies are presented in **Figure 3** and **Figure 4**. The halo masses M_h are given in the figure captions. For each simulation, the value of $\sigma(M_{\mathrm{PS}}, z, k_{\mathrm{fs}})$ (with a top-hat window function) is also given in the figure caption.

5. Non-Linear Regeneration of $P(k)$

Let us consider **Figure 1**. How probable is the density fluctuation (19) at $z_i = 65.9$? This density fluctuation has a Fourier transform (17) with a cut-off comoving wavevector $k_0 = 1.555/(2.72\ \mathrm{kpc}\cdot 66.9) = 8.6\ \mathrm{Mpc}^{-1}$. For our example (18), $k_{\mathrm{fs}} = 0.67\ \ \mathrm{Mpc}^{-1}$. The *linear* $P(k)$ is exponentially attenuated for $k > k_{\mathrm{fs}}$, so the density fluctuation in **Figure 1** is improbable. This is the argument in [2].

However, there are at least three phenomena not considered in [2]:

1. The linear power spectrum $P(k)$ of (11) develops a non-linear regenerated tail.

2. A majority of "small" galaxies have lost matter to their neighbors.

3. If dark matter particles are bosons that decouple while ultra-relativistic, *i.e.* are in thermal equilibrium with zero chemical potential while ultra-relativistic, then the excess of low momentum particles behaves as cold dark matter, see Figure 10 of [18].

The non-linear regeneration of $P(k)$ for warm dark matter is studied in [27]-[31]. We note, in Figure 4 of [28], or Figure 18 of [29], or Figure 4 of [31], that, if the ΛCDM power spectrum is cut-off by warm dark matter free-streaming, non-linear regeneration of $P(k)$ starts with first galaxies, and is a *major* first-order effect that should not be neglected! One of the origial reasons for considering warm dark matter is to reduce the counts of small galaxies with respect to the cold dark matter prediction that exceeds observations. This is the "missing satellites" problem. The suppression factor is obtained with warm dark matter simulations in [27]. Translating Equation (28) of [27] to our notation, we obtain

$$\frac{n_{\Lambda\mathrm{WDM}}(M_{\mathrm{PS}})}{n_{\Lambda\mathrm{CDM}}(M_{\mathrm{PS}})} = \left(1 + 0.61\frac{M_{\mathrm{fs}}}{M_{\mathrm{PS}}}\right)^{-1.16}. \tag{25}$$

From the *data* in Figures 1, Figures 2 and Figures 4 of [26] (for $z = 4,5$ or 6 that have sufficient data), we estimate the ratio of galaxy counts $n_{\mathrm{data}}(M_{\mathrm{PS}})/n_{\Lambda\mathrm{CDM}}(M_{\mathrm{PS}}) \approx 0.01$ at $M_{\mathrm{PS}} = 10^9\ \mathrm{M}_\odot$ (corresponding to **Figure 1**). From (25) we obtain the estimate $M_{\mathrm{fs}} \approx 9\times10^{10}\ \mathrm{M}_\odot$, corresponding to $k_{\mathrm{fs}} \approx 2$ Mpc^{-1}, $v_{h\mathrm{rms}}(1) \approx 170$ m/s, $m_h \approx 0.4$ keV, and $a_{h\mathrm{NR}} \approx 6\times10^{-7}$. This estimate of $a_{h\mathrm{NR}}$ is a factor ≈10 above the limit (4) and a factor ≈2.3 below the measurement (5).

Table 1. Tightest published lower limits on the "standard thermal relic" warm dark matter mass m_h obtained from different observables (from Figure 3 of [32]; see citations therein). Also shown is the corresponding upper limit on $a_{h\mathrm{NR}}$, and an approximate redshift of the measurements.

Observable	m_h	$a_{h\mathrm{NR}}$	Typical z
Milky way satellites	$\gtrsim 10$ keV	$\lesssim 2.3\times10^{-8}$	0
Strong lensing	$\gtrsim 6.0$ keV	$\lesssim 3.9\times10^{-8}$	0 to 1
Lyman-α forest	$\gtrsim 5.2$ keV	$\lesssim 4.5\times10^{-8}$	6
Galaxy UV luminosity distribution	$\gtrsim 3.2$ keV	$\lesssim 7.3\times10^{-8}$	6 to 8
γ ray burst	$\gtrsim 1.8$ keV	$\lesssim 1.3\times10^{-7}$	4 to 8

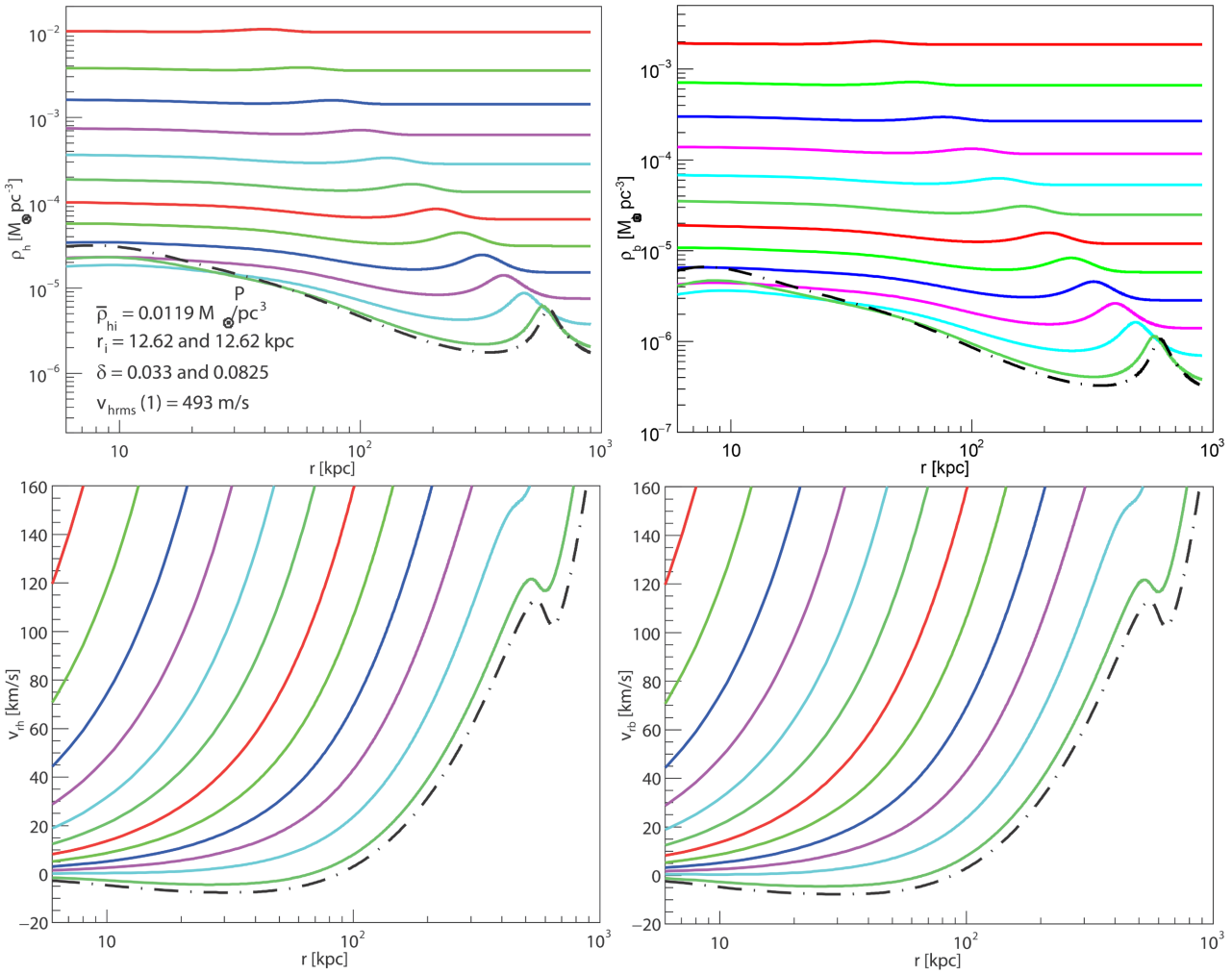

Figure 5. The dark matter and baryon densities and radial velocities are shown as a function of the proper radius r, at times that increase by factors $\sqrt{2}$ (except the last dashed line). The initial redshift of the numerical integration is $z_i = 65.9$. The parameters of this simulation of a "stripped-down" galaxy are $\bar{\rho}_{hi} = 0.0119\ \mathrm{M}_\odot/\mathrm{pc}^3$, $r_i = 12.625$ and 12.625 kpc, $\delta = 0.033$, and 0.08254, $v_{h\mathrm{rms}}(1) = 493$ m/s. The pivot point P has $r_{h\mathrm{P}} = 32$ kpc and $\rho_{h\mathrm{P}} = 1.3\times10^{-5}\ \mathrm{M}_\odot/\mathrm{pc}^3$. Initial $M_{\mathrm{PS}} = 10^{11}\ \mathrm{M}_\odot$. $M_h = 8\times10^9\ \mathrm{M}_\odot$. $\sigma(M_{\mathrm{PS}}, z_i, k_{\mathrm{fs}}) = 0.036$. $V_{\mathrm{rot}} = 27$ km/s.

Figure 3 of [32] summarizes published limits on m_h from several observables. The most stringent limit for each observable is presented in **Table 1**. These limits are obtained at $z \lesssim 8$ and so are sensitive to the regenerated power spectrum.

Consider the compilation of measurements of $P(k)$ in Figure 2 of [28]. The primordial linear power spectrum $P(k)$ at $z_{\text{dec}} = 1090$ is measured by the Planck mission for comoving wavevectors up to $k \lesssim 0.2$ Mpc^{-1}, *i.e.* does not reach warm dark matter free-streaming. All other measurements of $P(k)$ correspond to the regenerated power spectrum. A *direct* measurement of the linear $P(k)$ up to $k \approx 20$ Mpc^{-1}, before the first galaxies, will become possible with weak gravitational lensing of the cosmic microwave background (CMB) [28].

The observed reionization of the universe requires a delayed galaxy formation compared to the ΛCDM scenario. This delay requires $m_h = 0.51^{+0.22}_{-0.12}$ keV [33], or $k_{\text{fs}} \approx 2 \pm 1$ Mpc^{-1} [25], or $m_h = 1.3^{+0.3}_{-0.7}$ keV [34], or $m_h = 0.66^{+0.07}_{-0.08}$ keV [34]. These measurements are in tension with the limits in **Table 1** and can be compared with the measurements summarized in [4].

Small galaxies can develop due to the non-linear regeneration of small-scale structures, and also due to "stripping", *i.e.* loss of matter to neighbors.

6. Bottom-Up and Top-Down Evolution of Galaxies

Linear relative density perturbations are both positive and negative. Relative to a homogeneous universe, regions with under-density grow faster, and regions with overdensity grow slower, and peaks turn around and collapse into halos. The result is underdense regions, surrounded by sheets, that meet at filaments, that meet nodes where large galaxy clusters form. Galaxies punctuate the nodes and filaments, and to a lesser extent, the sheets and voids.

Let us try to understand the formation of small galaxy satellites. In the warm dark matter scenario, the first galaxies have masses determined by the warm dark matter free-streaming length, *i.e.*, a distribution of linear masses M_{PS} of order M_{fs}. The dark matter density $\rho_h(r)$ of these halos becomes equal to the mean dark matter density of the universe at a radius r_{max} that grows in proportion to $a^{3/2}$, faster than the separation between galaxies $\propto a$ [16]. Therefore, as the universe expands, groups of galaxies overlap and coalesce, becoming larger galaxies. Smaller galaxies become caught up between larger galaxies, loosing matter to their expanding neighbors, and are either absorbed completely, or collapse as "stripped-down" satellites with large cores (and continue loosing matter to their neighbors, perhaps leaving behind a globular cluster). Thus, in the warm dark matter scenario, the first galaxies have masses of order M_{fs}, and, from there on, the structure forms bottom-up and top-down, as confirmed by simulations [30].

Figure 1 of [35] can help us understand stripped-down galaxies. In the simulation of Figure 5 of [35], $M_{\text{fs}} = 3.6 \times 10^{11}\,\text{M}_\odot$ and $m_h = 0.112$ keV, similar to our example (18). We find that the number of stripped-down satellites per unit volume and a decade of mass, for a linear mass $M_{\text{PS}} \ll M_{\text{fs}}$, is reduced to ≈15% of the corresponding density in the ΛCMD cosmology (some, however, do not col-

lapse to a halo). Note that the Milky Way satellites are not formed as in Figure 1, but are stripped-down galaxies. The distribution of mass of stripped-down galaxies extends all the way to zero, and does not exclude the measurement (5).

The formation of a stripped-down galaxy is shown in Figure 5. This galaxy starts out as in Figure 4 with $M_{\rm PS} = 10^{11}\,{\rm M}_\odot$, but looses matter to neighbors (with spherical symmetry for convenience). The pivot point P has $r_{h\rm P} = 32$ kpc, and $\rho_{h\rm P} = 1.3\times10^{-5}\,{\rm M}_\odot/{\rm pc}^3$. So $\rho_{h\rm P} r_{h\rm P}^2 = 1.33\times10^4\,{\rm M}_\odot/{\rm pc}$, compared to $3.06\times10^4\,{\rm M}_\odot/{\rm pc}$ for the galaxy with no stripping in Figure 4. The parameters scale as

$$\rho_{h\rm P} r_{h\rm P}^2 \propto r_c^{-4}, \rho_{hc}^{2/3}, M_{hc}^{4/3}, M_{200}^{2/3}, r_{200}^2, \left\langle v_{hr}^2 \right\rangle, V_{\rm circ}^2. \tag{26}$$

So, with respect to the galaxy with no stripping in Figure 4, the core mass M_{hc} is reduced by a factor 0.54, $M_{200} \equiv M_h$ by a factor 0.29, and the circular velocity of a test particle is reduced by a factor 0.66.

A simple empirical way to account for both non-linear regeneration and stripped-down galaxies is to take

$$\tau^2(k) = \begin{cases} \exp\left(-\dfrac{k^2}{k_{\rm fs}^2}\right) & \text{if } k < k_{\rm fs}, \\ \exp\left(-\dfrac{k^n}{k_{\rm fs}^n}\right) & \text{if } k \geq k_{\rm fs}, \end{cases} \tag{27}$$

where n is *measured* to be in the range 0.5 to 1.1 [25]. This "tail" is sufficient to bring predictions in line with observations, see [26]. The effect of n on the predicted stellar mass distributions and on the ultra-violet luminosity distributions is presented in Figure 3 of [25].

Even the *linear* power spectrum $P(k)$ has a tail calculated in [18]. For our example in Section 5, with $k = 8.6\,{\rm Mpc}^{-1}$ and $k_{\rm fs} = 0.67\,{\rm Mpc}^{-1}$, we estimate $n \approx 1.08$ from Figure 10 of [18] for boson dark matter that decouples while ultra-relativistic (this is because the enhancement of low momentum bosons behaves like cold dark matter). In comparison, $\tau^2(k)$ of (9) has a tail corresponding to $n \approx 1.36$.

7. Conclusions

Warm dark matter free-streaming attenuates small-scale linear density perturbations. However, non-linear regeneration of small-scale structures is a major effect. Furthermore, a majority of galaxies with linear mass $M_{\rm PS} \ll M_{\rm fs}$ are stripped-down galaxies that have lost matter to neighbors. The limit (4), based on the observation of small Milky Way satellite galaxies, does not take regeneration, or stripping, into account. With the warm dark matter simulations in [27], an *estimate* of this limit becomes $a_{h\rm NR} \lesssim 6\times10^{-7}$, which is a factor ≈10 above the limit (4), and a factor ≈2.3 below the measurement (5). An empirical way to deal with non-linear regeneration and stripping is to add to $\tau^2(k)$ a "tail" as in (27). For the *measured* n [25], we obtain agreement with observed galaxy stellar mass dis-

tributions, and observed galaxy ultra-violet luminosity distributions, over a wide redshift range, down to $M_{\mathrm{PS}} = 5\times10^{8}\,\mathrm{M}_{\odot}$, or $M_{h} = 2\times10^{8}\,\mathrm{M}_{\odot}$, see [26]. So the minimum halo mass (6) is not excluded. Note that the mass distribution of stripped-down galaxies extends all the way to zero.

We are still far from a detailed and quantitative understanding of galaxy formation with warm dark matter. Each limit and measurement has its own issues, so caution and an open mind are called for. In any case, we are unable to rule out the *measurement* (5) beyond a reasonable doubt, in spite of all the published *limits* to the contrary.

All limits on k_{fs} that depend on galaxies need to include in the analysis the regeneration of small-scale structure, and the formation of stripped-down galaxies. Limits on k_{fs} from the Lyman-α forest need, in addition, to understand clouds of "left over" neutral hydrogen traces in the re-ionized universe [36]. On the other hand, measurements of $v_{h\mathrm{rms}}(1)$ with galaxy rotation curves are direct, but have the issue of relaxation that is constrained by observations, see [4] and references therein.

Acknowledgments

I thank Karsten Müller for his early interest in this work and for many useful discussions.

Conflicts of Interest

The author declares no conflicts of interest regarding the publication of this paper.

References

[1] Navas, S., *et al.* (Particle Data Group) (2024) Review of Particle Physics. *Physical Review D*, **110**, Article 030001.

[2] Lin, W., Chen, X., Ganjoo, H., Hou, L. and Mack, K.J. (2023) Cosmology of Single Species Hidden Dark Matter. arxiv:2305.08943.

[3] Hoeneisen, B. (2022) Measurement of the Dark Matter Velocity Dispersion with Dwarf Galaxy Rotation Curves. *International Journal of Astronomy and Astrophysics*, **12**, 363-381. https://doi.org/10.4236/ijaa.2022.124021

[4] Hoeneisen, B. (2024) Measurements of the Dark Matter Mass, Temperature and Spin. *International Journal of Astronomy and Astrophysics*, **14**, 184-202. https://doi.org/10.4236/ijaa.2024.143012

[5] Lin, W. and Ishak, M. (2016) Ultra Faint Dwarf Galaxies: An Arena for Testing Dark Matter versus Modified Gravity. *Journal of Cosmology and Astroparticle Physics*, **10**, Article 025. https://doi.org/10.1088/1475-7516/2016/10/025

[6] Nadler, E.O., Gluscevic, V., Boddy, K.K. and Wechsler, R.H. (2019) Constraints on Dark Matter Microphysics from the Milky Way Satellite Population. *The Astrophysical Journal Letters*, **878**, L32. https://doi.org/10.3847/2041-8213/ab1eb2

[7] Ludlow, A.D., Bose, S., Angulo, R.E., Wang, L., Hellwing, W.A., Navarro, J.F., *et al.* (2016) The Mass-Concentration-Redshift Relation of Cold and Warm Dark Matter Haloes. *Monthly Notices of the Royal Astronomical Society*, **460**, 1214-1232. https://doi.org/10.1093/mnras/stw1046

[8] Benson, A.J., Farahi, A., Cole, S., Moustakas, L.A., Jenkins, A., Lovell, M., *et al.* (2013) Dark Matter Halo Merger Histories Beyond Cold Dark Matter-I. Methods and Application to Warm Dark Matter. *Monthly Notices of the Royal Astronomical Society*, **428**, 1774-1789. https://doi.org/10.1093/mnras/sts159

[9] Avila-Reese, V., Colin, P., Valenzuela, O., D'Onghia, E. and Firmani, C. (2001) Formation and Structure of Halos in a Warm Dark Matter Cosmology. *The Astrophysical Journal*, **559**, 516-530. https://doi.org/10.1086/322411

[10] Macciò, A.V., Ruchayskiy, O., Boyarsky, A. and Muñoz-Cuartas, J.C. (2012) The Inner Structure of Haloes in Cold + Warm Dark Matter Models. *Monthly Notices of the Royal Astronomical Society*, **428**, 882-890. https://doi.org/10.1093/mnras/sts078

[11] Gilman, D., Birrer, S., Nierenberg, A., Treu, T., Du, X. and Benson, A. (2020) Warm Dark Matter Chills out: Constraints on the Halo Mass Function and the Free-Streaming Length of Dark Matter with Eight Quadruple-Image Strong Gravitational Lenses. *Monthly Notices of the Royal Astronomical Society*, **491**, 6077-6101. https://doi.org/10.1093/mnras/stz3480

[12] Nadler, E.O., Mao, Y., Green, G.M. and Wechsler, R.H. (2019) Modeling the Connection between Subhalos and Satellites in Milky Way-Like Systems. *The Astrophysical Journal*, **873**, Article 34. https://doi.org/10.3847/1538-4357/ab040e

[13] Jethwa, P., Erkal, D. and Belokurov, V. (2018) The Upper Bound on the Lowest Mass Halo. *Monthly Notices of the Royal Astronomical Society*, **473**, 2060-2083. https://doi.org/10.1093/mnras/stx2330

[14] Weinberg, S. (2008) Cosmology. Oxford University Press.

[15] Hoeneisen, B. (2023) Understanding the Formation of Galaxies with Warm Dark Matter. *Journal of Modern Physics*, **14**, 1741-1754. https://doi.org/10.4236/jmp.2023.1413103

[16] Hoeneisen, B. (2025) Why Do Galaxies Have Extended Flat Rotation Curves? *International Journal of Astronomy and Astrophysics*, **15**, 1-10. https://doi.org/10.4236/ijaa.2025.151001

[17] Viel, M., Lesgourgues, J., Haehnelt, M.G., Matarrese, S. and Riotto, A. (2005) Constraining Warm Dark Matter Candidates Including Sterile Neutrinos and Light Gravitinos with WMAP and the Lyman-α Forest. *Physical Review D*, **71**, Article 063534. https://doi.org/10.1103/physrevd.71.063534

[18] Boyanovsky, D., de Vega, H.J. and Sanchez, N.G. (2008) Dark Matter Transfer Function: Free Streaming, Particle Statistics, and Memory of Gravitational Clustering. *Physical Review D*, **78**, Article 063546. https://doi.org/10.1103/physrevd.78.063546

[19] Piattella, O.F., Rodrigues, D.C., Fabris, J.C. and de Freitas Pacheco, J.A. (2013) Evolution of the Phase-Space Density and the Jeans Scale for Dark Matter Derived from the Vlasov-Einstein Equation. *Journal of Cosmology and Astroparticle Physics*, **11**, Article 002. https://doi.org/10.1088/1475-7516/2013/11/002

[20] Mistele, T., McGaugh, S., Lelli, F., Schombert, J. and Li, P. (2024) Radial Acceleration Relation of Galaxies with Joint Kinematic and Weak-Lensing Data. *Journal of Cosmology and Astroparticle Physics*, **4**, Article 020. https://doi.org/10.1088/1475-7516/2024/04/020

[21] Munshi, F., Brooks, A.M., Applebaum, E., Christensen, C.R., Quinn, T. and Sligh, S. (2021) Quantifying Scatter in Galaxy Formation at the Lowest Masses. *The Astrophysical Journal*, **923**, Article 35. https://doi.org/10.3847/1538-4357/ac0db6

[22] Press, W.H. and Schechter, P. (1974) Formation of Galaxies and Clusters of Galaxies by Self-Similar Gravitational Condensation. *The Astrophysical Journal*, **187**, 425-438.

https://doi.org/10.1086/152650

[23] Sheth, R.K. and Tormen, G. (1999) Large-Scale Bias and the Peak Background Split. *Monthly Notices of the Royal Astronomical Society*, **308**, 119-126. https://doi.org/10.1046/j.1365-8711.1999.02692.x

[24] Sheth, R.K., Mo, H.J. and Tormen, G. (2001) Ellipsoidal Collapse and an Improved Model for the Number and Spatial Distribution of Dark Matter Haloes. *Monthly Notices of the Royal Astronomical Society*, **323**, 1-12. https://doi.org/10.1046/j.1365-8711.2001.04006.x

[25] Hoeneisen, B. (2022) Measurement of the Dark Matter Velocity Dispersion with Galaxy Stellar Masses, UV Luminosities, and Reionization. *International Journal of Astronomy and Astrophysics*, **12**, 258-272. https://doi.org/10.4236/ijaa.2022.123015

[26] Hoeneisen, B. (2024) Are James Webb Space Telescope Observations Consistent with Warm Dark Matter? *International Journal of Astronomy and Astrophysics*, **14**, 45-60. https://doi.org/10.4236/ijaa.2024.141003

[27] Schneider, A., Smith, R.E., Macci'o, A.V. and Moore, B. (2012) Nonlinear Evolution of Cosmological Structures in Warm Dark Matter Models. arxiv:1112.0330.

[28] MacInnis, A., and Sehgal, N. (2024) CMB-HD as a Probe of Dark Matter on Sub-Galactic Scales. arxiv:2405.12220.

[29] Despali, G., Moscardini, L., Nelson, D., Pillepich, A., Springel, V. and Vogelsberger, M. (2025) Introducing the AIDA-TNG Project: Galaxy Formation in Alternative Dark Matter Models. *Astronomy & Astrophysics*, **697**, A213. https://doi.org/10.1051/0004-6361/202553836

[30] Paduroiu, S., Revaz, Y. and Pfenniger, D. (2015) Structure Formation in Warm Dark Matter Cosmologies Top-Bottom Upside-Down. arxiv:1506.03789.

[31] Parimbelli, G., Scelfo, G., Giri, S.K., Schneider, A., Archidiacono, M., Camera, S., *et al.* (2021) Mixed Dark Matter: Matter Power Spectrum and Halo Mass Function. *Journal of Cosmology and Astroparticle Physics*, **12**, Article 044. https://doi.org/10.1088/1475-7516/2021/12/044

[32] Liu, B., Shan, H. and Zhang, J. (2024) New Galaxy UV Luminosity Constraints on Warm Dark Matter from JWST. *The Astrophysical Journal*, **968**, Article 79. https://doi.org/10.3847/1538-4357/ad4ed8

[33] Lin, H., Gong, Y., Yue, B. and Chen, X. (2024) Implications of the Stellar Mass Density of High-Z Massive Galaxies from JWST on Warm Dark Matter. *Research in Astronomy and Astrophysics*, **24**, Article 015009. https://doi.org/10.1088/1674-4527/ad0864

[34] Lapi, A., Ronconi, T., Boco, L., Shankar, F., Krachmalnicoff, N., Baccigalupi, C., *et al.* (2022) Astroparticle Constraints from Cosmic Reionization and Primordial Galaxy Formation. *Universe*, **8**, Article 476. https://doi.org/10.3390/universe8090476

[35] Hoeneisen, B. (2019) Simulations and Measurements of Warm Dark Matter Free-Streaming and Mass. *International Journal of Astronomy and Astrophysics*, **9**, 368-392. https://doi.org/10.4236/ijaa.2019.94026

[36] Keating, L.C., Puchwein, E. and Haehnelt, M.G. (2018) Spatial Fluctuations of the Intergalactic Temperature-Density Relation after Hydrogen Reionization. *Monthly Notices of the Royal Astronomical Society*, **477**, 5501-5516. https://doi.org/10.1093/mnras/sty968